Morphological Tunability of the Plasmonic Response: From Hollow Gold Nanoparticles to Gold Nanorings

Martin Prieto[a,$], Raul Arenal[*b,c,$], Luc Henrard[d,$], Leyre Gomez[a,e],Victor Sebastian[a,e], Manuel Arruebo[,a,e]*

[a]Department of Chemical Engineering and Aragon Nanoscience Institute (INA), EdificioI+D+i, C/Mariano Esquillor s/n, University of Zaragoza, 50018 Zaragoza, Spain.

[b]Laboratorio de Microscopias Avanzadas, Instituto de Nanociencia de Aragón, Universidad de Zaragoza, 50018 Zaragoza, Spain.

[c]ARAID Foundation, 50018 Zaragoza, Spain.

[d]Department of Physics, University of Namur. 61, rue de Bruxelles, 5000 Namur, Belgium.

[e]Networking Research Center on Bioengineering, Biomaterials and Nanomedicine, CIBER-BBN, 50018 Zaragoza, Spain.

*Email: arenal@unizar.es ; arruebom@unizar.es

[$]Equal contribution.

1

Abstract:

The optical and morphological properties of hollow gold nanoparticles (HGNPs) can be finely modified by employing Poly-L-Lysine hydrobromide (PLL), an homo poly aminoacid of the L-lysine, used as reducer and stabilizer. We demonstrate that the reshaping of these plasmonic hollow nanostructures responds to an Ostwald ripening process in which the initial HGNPs dissolve under the acidic conditions provided by the PLL generating chloroaurate ions. These ions are then reduced by the primary amines of the PLL itself to produce metallic gold which is then re-deposited on the surface of the HGNPs rendering the final shape; either nanorings or even spheres depending on the contact time. We investigate locally the plasmonic response of these nanostructures by electron energy loss spectroscopy (EELS). The plasmon excitations are interpreted by discrete dipole approximation (DDA) simulations. We demonstrate that thanks to this controlled top-down morphological modification a fine tuning of the optical response is possible. Unlike the traditional lithographic techniques, this has been achieved in a controlled manner using wet chemistry, enabling the potential use of these nanostructures for a broad range of plasmonic applications, including biomedicine, catalysis and quantum communications.

2

Introduction.

Hollow gold nanoparticles are interesting plasmonic nanostructures showing collective electron charge oscillations named localized surface plasmons resonances (SPR) which can exhibit enhanced near-field amplitude at the resonance frequency[1]. Those nanomaterials are widely used in catalysis, medicine, sensing and photonics. In catalysis, compared to solid nanoparticles, they show enhanced catalytic properties due to the cage effect by confining the reactants inside their hollow interiors and those inner crystalline facets show a superior catalytic activity[2]. In medicine, therapeutic and diagnostic applications benefit from their plasmonic response. In therapy, they are used in cancer treatment as transductors of the absorbed near infrared light into heat causing selectively cellular death in the nanoshell-laden cells[3] or they can also be used to trigger the release of therapeutic molecules in drug[4] or gene[5] delivery applications. Those hollow structures show improved properties such as prolonged blood circulation half-life compared to other NIR absorbing nanoparticles including core/shell SiO_2/Au nanoparticles[6] and they also show less cytotoxicity than gold nanorods[7]. In diagnosis, they are used as photoacustic imaging tags[8], as contrast agents in optical coherence tomography[9, 10] and in multi-photon microscopy[11]. They also can be used as biosensors[12] and thermal tags[13].

Galvanic replacement[14,15,16] is the most common synthesis protocol used for the synthesis of those hollow gold nanoparticles, in which a sacrificial metal (i.e., Ag or Co) is oxidized at the same time that a gold (III) salt is reduced on it generating a hollow Au shell because the reduction potential of $AuCl_4^-$/Au (0.99 V vs. SHE) is more positive than that of AgCl/Ag (0.22 V vs. SHE) or

Co^{2+}/Co (-0.28 V vs. SHE). Different reductors and/or stabilizers are used during the synthesis including polyvinylpyrrolidone (PVP)[2, 9, 17], citrate groups[3, 5], hexadecyltrimethyl ammonium bromide[18], and so on. After synthesis and for those applications in which the resulting nanoparticles could be subjected to biofouling (i.e., opsonization) pegylation is commonly carried out by means of thiol- or amino-PEG taking advantage of the strong chemical bond between gold and sulphur[19] or nitrogen[20], respectively. Guo et al.[21] reported that a single dose of those hollow nanostructures show long term stability under physiological conditions remaining within Kupffer cells 3 months after i.v. administration. However, Goodman et al.[22] showed recently that the same nanostructures were unstable and prone to fragmentation under physiological conditions when fetal bovine serum was added to the media and that acidic media destroyed the nanoparticles even after pegylation. They attributed such destruction to the presence of Ag (used in the galvanic replacement) on the surface of the hollow gold nanoparticles and to the protein corona formed around the nanoparticles which could have a destructive effect. Considering those observations we evaluated in this work the morphological changes of those nanostructures under different pHs and under the presence or absence of an amino-based reducing agent (Poly-L-Lysine Hydrobromide) and a surface protective PEG when using cobalt as sacrificial template with the goal of understanding their plasmonic response and stability under those different conditions. In addition, we investigate the way for tuning the plasmonic response of those nanoparticles as function of the pH of the reactions taking place and the presence of amines as reductive agents.
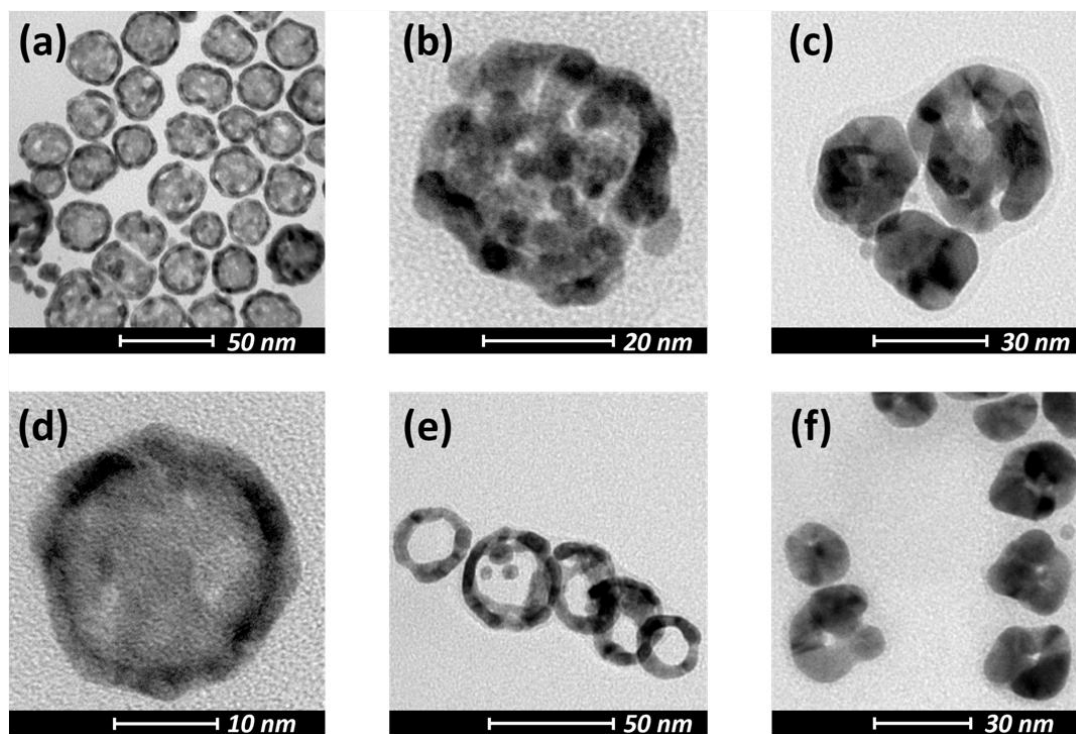
Electron energy loss spectroscopy (EELS) carried out in a transmission electron microscope (TEM) is a very powerful technique for investigating the optical response of materials at local scale[23-30]. In the present work, we have studied two different kinds of Au nanostructures (gold

4

hollow spheres and nanorings) via low-loss EELS experiments using a probe-corrected and monochromated TEM. Particular attention has been paid to the different parameters (size/aspect-ratio, shape and dielectric environment) influencing the SPR response of these materials. Our interpretation is based on discrete dipole approximation (DDA) simulations. Furthermore, the precise composition, geometry and atomic structure of the nanoparticles have been carefully studied by energy-dispersive X-ray spectroscopy (EDS) and high-angle annular dark field using high/resolution scanning TEM (HAADF-HRSTEM) measurements. Our studies demonstrate that the fine control of the optical response of these objects is possible and it can be precisely monitored by local probe measurements. While many of the nanorings' synthesis protocols are based on top-down approaches (i.e., colloidal lithography[31]); here we describe how by following a bottom-up approach it is possible to control the geometry of the transitions between hollow gold nanoparticles and nanorings as requested by other authors[32].

Results and discussion

We have observed a strong morphological modification of the gold NPs as a function of the pH of an added HCl solution, see Figure 1. At pH 7, the Au nanoparticles have a stable and uniform hollow spherical morphology (HRTEM of Fig. 1 (a) and (b)), but at pH 2 the shape of the NPs changes significantly, becoming a sort of distorted nano-torus/-ring or polycrystalline compact NP, see Fig. 1 (c). An intermediated step, at pH 5, shows Au sphere-like NP, formed as a sort of decomposition of the original HGNPs, Fig. 1 (b). It is already known that acidic media promotes the de-alloying of the shell when using silver as sacrificial templates which is responsible of fragmentation[22]. In addition, adding $HAuCl_4$ to the HGNPs produces the replacement of the

5

remaining silver resulting in reconstruction and formation of pinholes and ultimately leading to fragmentation[18]. In our case, when using cobalt as sacrificial template instead of silver as in the previous references, we also observe fragmentation and de-alloying. These effects are the responsible for these morphological changes.
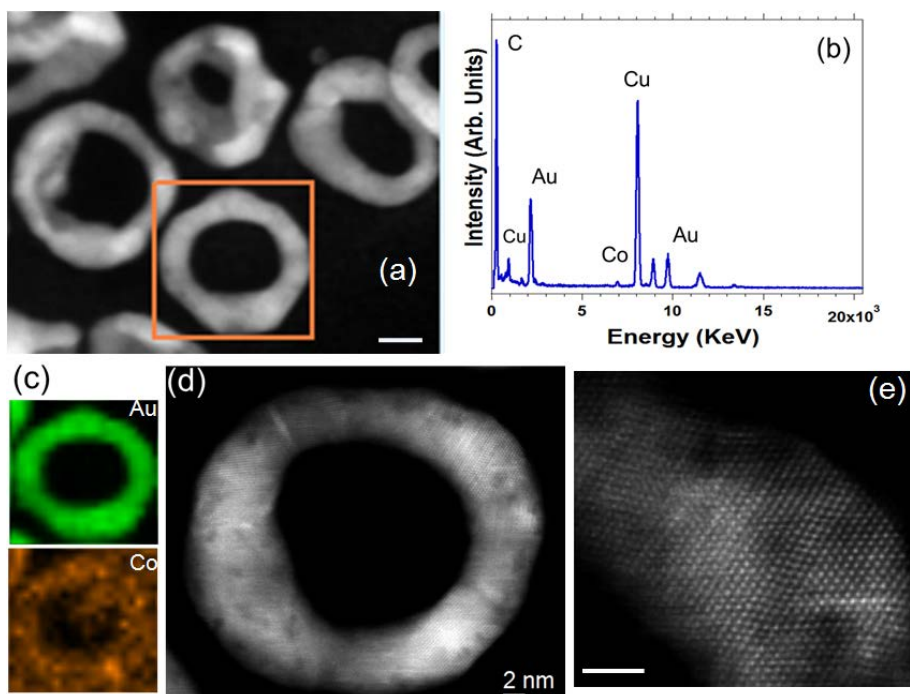

Figure 1.(a) – (c) Conventional TEM images characteristic of samples of aqueous dispersions of HGNPs at different pHs: 7, 5 and 2, respectively. pH modification was achieved by adding increased amounts of HCl. (d) – (f) Conventional TEM images characteristic of samples of aqueous dispersions of 1:1 Poly-L-Lysine Hydrobromide: HGNPs (0,5 mg/mL),corresponding to (d) initial, (e) after 2 h of reaction time (pH = 5) and (f) after 28 h of reaction time (pH = 5).

Upon addition of Poly-L-Lysine Hydrobromide on these HGNPs, there is another very interesting morphological modification. During this treatment, the pH of the dispersion rapidly decreases to 5 due to the acidic character of the PLL with a consequent reshaping from HGNPs to

6

gold nanorings, Fig.1 (e)-(f). It is important to point out that Poly-L-Lysine Hydrobromide acts simultaneously as an acid due to its nature and as a reductor due to the large amount of primary amines present, and that only pH reduction does not allow controlling the morphology of the final nanoparticles and consequently their plasmonic response. As we will see below, this characteristic reshaping was analyzed over time in order to control the plasmonic response of the original HGNPs by the combination effect of the acidic environment provided by the Hydrobromide together with the reductive action of the primary amines in the side chains of the Poly-L-Lysine. Indeed, after 28h of reaction, the nanorings (NR) underwent a morphological change and reshaped into spherical or pinhole nanoparticles with a progressive decrease in the aspect ratio of the walls of the intermediated nanoring formed after 2h of reaction time.

We turn now to the detailed elemental and structural analyses that we have carried out in these nanorings, see Figure 2. We have developed nanometer-resolved X-ray electron dispersive spectroscopy (X-EDS) for obtaining the local chemical information of these nanostructures, Fig. 2 (a)-(c). The elemental analyses show that these NR are composed of Au, but few amounts of Co are also present, see Figure 2 (b) and (c). A X-EDS spectrum-image (SPIM) has been recorded on the area marked in the HAADF-STEM image of Fig. 2 (a). A selection of 12 EDS spectra are depicted in Fig. 2 (b). C-K and Cu-K and Cu-L shell-lines are visible in this EDS sum spectrum. They correspond to the TEM grid used for these microscopic studies which is a carbon film supported on a Cu mesh grid. The elemental maps of Au and Co (Fig. 2(c)) have been extracted from the EDS spectrum-image recorded in Fig. 2 (a), analyzing the Au-M and Co-K shell-lines, respectively. This small amount of Co remains from the production of the NR, because, as discussed above, the cobalt has been used as sacrificial template. In addition, the HAADF-HRSTEM micrographs, recorded on

7

other Au nanoring and displayed in Fig. 2 (d) and (e), confirm the good crystalline quality of these NR.

Figure 2. (a) HAADF image of several nanorings. An X-EDS spectrum-image (SPIM) has been recorded in the rectangular area marked in the image. Scale bar 10 nm. (b) Sum of 12 EDS spectra selected from the rectangular marked area in red in Fig. 2 (a). Carbon, copper (both of these elements come from the TEM grid), gold and cobalt are visible in this spectrum. (c) and (d) Au and Co maps extracted from this EDS spectrum-image, respectively. (d) and (e) Two HAADF-HRSTEM micrographs recorded on another Au nanoring. Scale bar in (e) 2 nm.

A potential mechanism, which explains the transition between a nanoring to an almost closed spherical particle would depend on, the protonation state of the amines present. We postulate that in a first stage the HGNPs would dissolve under the acidic conditions provided by the PLL, releasing $AuCl_4^-$ to the media. Then this ion could bind to an amine either by ligand exchange with a neutral amine changing the Au-Cl coordination number or by forming an ion pair with a protonated amine

8

without any change in the Au-Cl coordination number[33]. The capability of amines to be neutral and protonated at the same time has been previously observed and attributed to the observation of pKa shifts (up to 5 pH units) when they are confined in cavities due to their high density and restricted mobility within a confined space[33]. In addition, primary amines of linear polymers have lower pKas than expected because of suppression of protonation by closely spaced charged groups[34]. Therefore, the neutral amine would reduce the chloroaurate ion, obtained after an initial gold-nanoring dissolution, by transferring electrons to the metal ion, forming Au(0) and resulting an almost closed sphere from the initial gold nanoring according to the chemical reaction (Eq 1):

Eq.1 $\qquad$ $HAuCl_4 + 3NR_3 \rightarrow Au^0 + 3NR_3^+ + H^+ + 4Cl^-$

Indeed, the reduction of chloroaurate ions to Au(0) is a three electron process requiring three nitrogen atoms from the primary amines in the side chains of the Poly-L-Lysine to each function as one-electron reducing agent (see Scheme 1 in the Supp. Info.). This shape transition was exclusively achieved after the combined effect of the acidic media and the reductive capacity of the PLL. Only pH does not have any reshaping ability besides an induction of fragmentation.
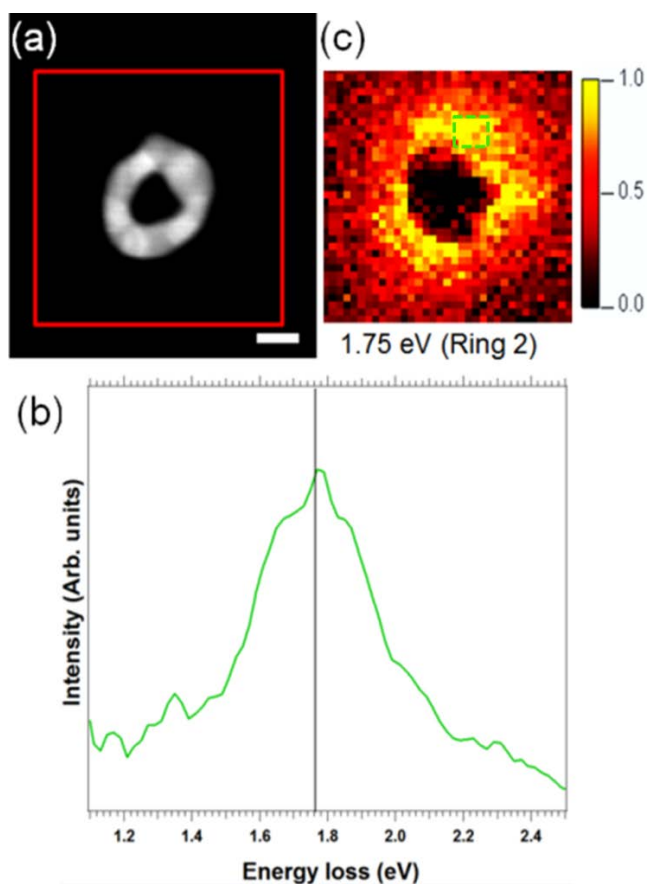
In summary a concurrent effect of acidic pH and PLL addition caused a red-ox reaction that resulted in a nanoparticle reshape from hollow nanoparticles to nanorings in a first stage. PLL in aqueous solution has a pH close to 4 being protonated under those conditions. Therefore, part of the hollow gold nanoparticle dissolves producing $AuCl_4^-$ ions which are then reduced to render rings due to the characteristic reductive effect of the amines in the Poly-L-Lysine which transfer electrons. $AuCl_4^-$ ions reduce to Au(0) forming a ring whereas the Poly-L-Lysine is oxidized. In a second stage the nanoring can reshape again into pinhole or spherical nanostructures following the same mechanism due to the presence of those cationic polyelectrolytes with amino side-groups, which

9

rapidly reduce cloroaurate ions. In Suppl. Info., Fig. S1 displays several HAADF images illustrating these morphological transformations. These processes of reshaping are probably caused by an Ostwald ripening process due to the initial dissolution under acidic conditions and a secondary re-deposition process rendering the final shape. Given that the as-grown polycrystalline hollow gold nanoparticle or nanorings are metastable nanostructures, and then they are not the most thermodynamically favored morphologies, they should be in a certain extent susceptible to reshaping. Particularly, the polycrystalline surface of the metastable nanostructures makes them sensitive to any reactivity specific to certain crystallographic facets. Then, during anisotropic Ostwald ripening, the growth of certain crystallographic facets is favored at the expense of the dissolution of other more unstable[35]. For instance, the higher energy density of the inner facets at the HGNPs pinholes or the nanoring can favor the re-deposition of the dissolved Au atoms to a more stable morphology, which is a spherical shape.

For better understanding this transformation mechanism the surface of the HGNPs was protected with PEG by using monofunctional thiol-PEG carrying out a covalent coupling between the HGNPs and the thiol groups of the PEG. Under those conditions a slight blue shift in the extinction peak after pegylation was observed (see Supporting information), probably caused by the slight modification in the dielectric constant of the media in agreement with the previous literature[22]. After PLL addition and 28 h after reaction the characteristic plasmon peak of the PEGylated HGNPs remained unaltered, indicative of the protective shielding effect of the PEG against the reductive action of the PLL. Therefore, Ostwald ripening can be avoided by using protective polymers on the surface of gold nanostructures in agreement with the previous literature[36]. The stability of the resulting nanostructures was also assured by analyzing the results of the zeta potential measurements

10

for the resulting colloids (see Supporting information) where large electrostatic repulsion together with the steric hindrance introduced by the PEG guaranteed colloidal stability.

The reductive effect of other amines at the same concentration including L-lysine, Poly-D-Lysine and BSA was also studied. The reductive capacity of BSA and Poly-D-Lysine were able to reduce and reshape the initial HGNP-based dispersion in the same fashion as Poly-L-Lysine did, but the red-ox potential of L-lysine was insufficient to reshape those HGNPs. Due to the higher pH provided by the BSA solution the process was slower compared to the L or D- PLL. No differences were observed when using Poly-L-Lysine of different molecular weights (results not shown).
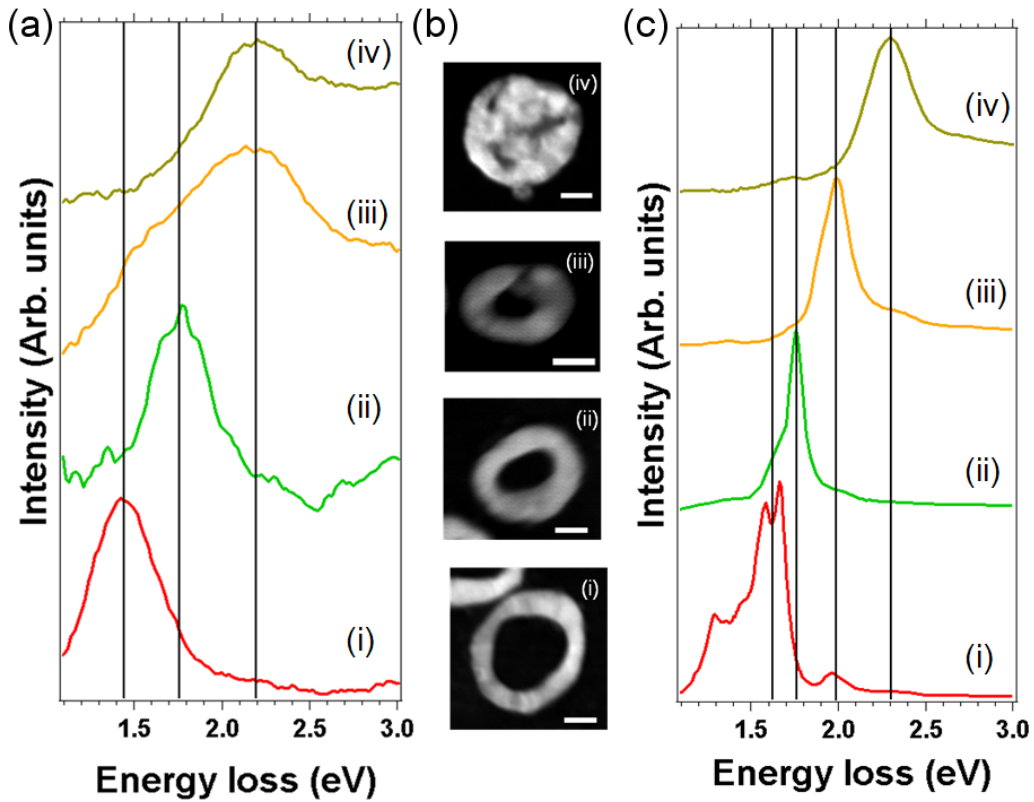
Figure 3. (a) HAADF-STEM image (scale bar 10 nm) of an Au nanoring, where an EELS SPIMs has been recorded in the red marked area. **(b)** EEL spectrum, after background subtraction, corresponding to the sum of 12 spectra collected from the green marked area of Fig. 3 (c). **(c)** Intensity maps showing the spatial distribution of the SPR mode (1.75 eV.) for this Au NR.

As mentioned above, the local surface plasmon resonances (LSPR) depend on the shape, size and dielectric environment of the probed nano-object. We have investigated these effects and we have carried out systematic local EELS-TEM analyses on different kind of nanoparticles: hollow spheres and nanorings with different aspect-ratios/sizes. Figure 3 (a) displays the HAADF image of a NR. An EELS-SPIM has been recorded on the marked red area. A typical EEL spectrum (sum of 12 spectra) is plotted in Fig. 3 (b). This spectrum has been extracted from the green area marked on the intensity map displayed in Fig. 3 (c). The map corresponds to the intensity of the SPR mode at 1.75 eV extracted for the SPIMs after zero-loss peak (ZLP) subtraction (see Methods Section). In NR, there is a significant coupling between the two electromagnetic modes of the inner and outer surfaces of the nanostructures, leading to dipolar symmetric and antisymmetric plasmon modes.[31,37] Only the symmetric mode is observed because of its dominant excitation cross section of excitation by light or by electrons. The coupling (or hybridization) is directly related to the aspect ratio ($\sigma = $ d/0.5D, where "d" and "D" are the wall thickness and the diameter of the NR, respectively) dependence of the LSPR, as predicted and observed by optical measurements.[31] A further coupling of the 15 nm height NR with the substrate (Si_3N_4 film, thickness 15nm) also led to a redshift of the plasmon modes compared to isolated self-supported NR.

We have also analyzed the aspect ratio and the morphology effects on the plasmonic behaviors of the NR and HGNPs of different dimensions. A selection of EEL spectra, after ZLP

12

subtraction and each of them corresponding to the sum of 8-12 spectra, is displayed in Fig. 4 (a). These EEL spectra have been recorded on the NR and HGNPs showed in Fig. 4 (b) and noted as (from bottom to top, (i) to (iv)) Ring 1, Ring 3, Ring 6 and Sphere 1. The geometric parameters are given in the Table 1, DDA EELS simulations[29,41] for the corresponding (same sizes/aspect ratios) NPs are presented in Fig. 4(c) and in the right column of the table. In the simulations, a Si_3N_4 substrate is considered. Additional experiments and simulations are provided in the Suppl. Info. A very good agreement of the plasmon modes energies is found. The larger width of the experimental data is related to the unregular shape of the NR (see HAADF images).

Figure 4. (a) EEL spectra (each of them corresponds to the sum of 8-12 spectra, after background subtraction) recorded on nanorings of different aspect ratios (σ), (see table 1) ring 1 (i), ring 3 (ii), ring 6 (iii) and hollow sphere (iv). (b) HAADF images of the corresponding nanostructures. Scale
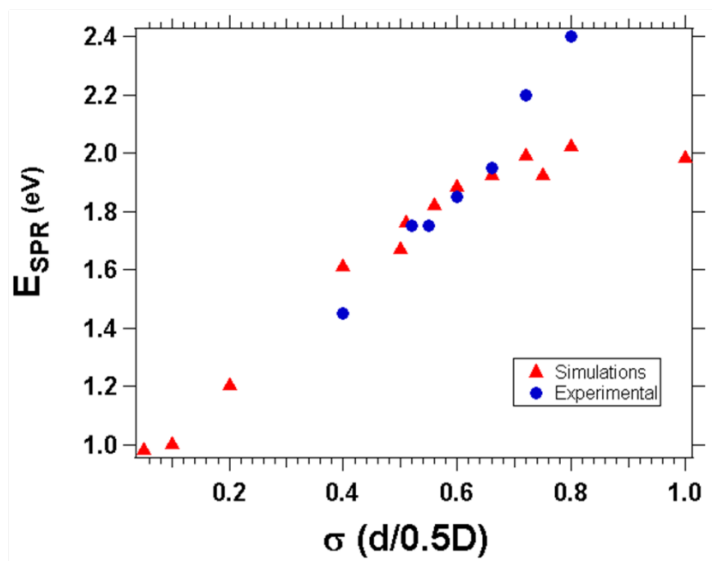
bar is 10 nm for all these micrographs. (c) EELS DDA simulations for the corresponding (same sizes) NPs.

The σ dependence is further evidenced on Table 1 and Fig. 5 where the experimental and simulated EELS plasmon modes energies are displayed. The σ dependence reproduces the results of Aizpurua et al.[31], i.e., confirming that the SPR coupling is more pronounced for small σ. We note that we directly simulated EELS spectra in the present work, where only optical absorption was considered in the work of Aizpurua et al.[31] and, more importantly, tabulated 'real' dielectric data of gold has been considered rather than a Drude model (see Suppl. Info. for more details). It is worth mentioning that the height of these NP (~ 15 nm) is very homogeneous for all these nanorings, and then it is not playing a significant effect on the observed SPR shifts. However, the large width of the experimental LSPR is related to the slight irregular shape of the NR. The irregular shape also makes difficult the assignment of a single thickness (d) (and then a single□ σ) to each NR. This shape irregularity explains the minor differences between simulated and experimental curves. In particular, rings with small σ (as for instance, ring 1, curve (i) on Fig. 4) are very sensitive to the exact geometry.[31]

Table 1. Experimental data and simulations of SPR energies and morphology of several gold hollow spherical nanoparticles and nanorings. (*) This nanoring is only partially supported on the substrate (see text).

14

Size / SPRs / Shape	Diameter (D)	Thickness (d)	σ (d/0.5D)	SPR – Energy (Experim.)	SPR – Energy (Theo. Vac.)	SPR – Energy (Theo. Si_3N_4)
Sphere 1	40 nm	7.5 nm	0.38	2.20 eV	2.35 eV	2.30 eV
Sphere 2	40 nm	8 nm	0.4	2.30 eV	2.35 eV	2.30 eV
Ring 1	40 nm	8.0 nm	0.4	1.45 eV	1.95 eV	1.60 eV
Ring 2	30 nm	8.5 nm	0.55	1.75 eV	2.20 eV	1.80 eV
Ring 3	35 nm	9.0 nm	0.52	1.75 eV	2.15 eV	1.75 eV
Ring 4	30 nm	9.0 nm	0.6	1.85 eV	2.20 eV	1.90 eV
Ring 5	30 nm	10 nm	0.66	1.95 eV	2.25 eV	1.95 eV
Ring 6	25 nm	9.0 nm	0.72	2.20 eV	2.30 eV	2.00 eV
Ring 7 *	25 nm	10 nm	0.8	2.40 eV *	2.35 eV *	2.00 eV *

Ring 7 ($\sigma = 0.8$) presents a LSP resonance at 2.40 eV, which much larger than the 2 eV predicted by simulations (Table 1 and Fig. 5). This discrepancy is explained by the fact that this nanoring is only partially supported on the Si_3N_4 substrate, being most part of the particle on the vacuum (see Fig. S2 in Suppl. Info.). Isolated NR with the same morphology with no substrate interaction present a dipolar SPR calculated at 2.35 eV, very close to the observed one.

15

Figure 5. Dispersion of SPR modes as a function of the aspect ratio of the Au NR and Au HGNP. Experimental data (blue circles) are those of Table 1. Simulation data (red triangles) are those for the same morphology/dimensions. Other data are added for the simulation points (see Suppl. Info.).

Conclusions

In summary, morphological reshaping of hollow gold nanoparticles to gold nanorings or to almost spherical nanoparticles has been obtained by using PLL, which reduces the pH resulting colloidal chloroaurate ions. In addition, PLL has also a strong reductive action on the dissolved ions to produce gold nanorings or almost closed nanostructures depending on the contact time. We have monitored, by local EELS measurements, these morphological modifications and their dependence on the surface plasmon modes. In particular, we have followed the shift of the dipolar mode of the gold nanorings as a function of their aspect ratio. All these findings have been supported by DDA calculations which also helped to elucidate these observed behaviours. These results demonstrate

16

that a fine tune of the plasmonic response of Au NPs is achievable, offering the possibility of applying these NPs on different fields as sensing, photonics and catalysis.

Materials and Methods

Materials:

Hollow Gold Nanoparticles (HGNPs) have been synthesized via galvanic replacement of cobalt with gold as previously reported by Preciado-Flores et al.[17]. Briefly, 100µL of 0.4 M cobalt chloride hexahydrate ($CoCl_2 \cdot 6H_2O$) and 400 µL of 0.1 M sodium citrate dihydrate ($Na_3C_6H_5O_7 \cdot 2H_2O$) were mixed in a round-bottom flask with 100 mL of distillated water. All the chemicals were purchased from Sigma Aldrich and used as supplied. The solution was deareated by bubbling with argon for 40 min. 500 µL of a 1 wt.% solution of poly(vinylpyrrolidone) (PVP) with an average molecular weight of 55000 Da and 100 µL of 0.1 M sodium borohydride ($NaBH_4$) were injected under magnetic stirring to the previously deareated solution. The solution turned from a pale pink to dark brown in a few seconds indicating the formation of cobalt NPs. This dispersion was maintained under magnetic stirring and argon bubbling for a further 40 min to complete the hydrolysis of the sodium borohydride. Subsequently, 30 mL of this cobalt nanoparticle dispersion was transferred to a stirred solution of 10 mL of distillated water with 15 µL of 0.1 M $HAuCl_4$ allowing the formation of $CoCl_2$, CoO and the reduction of Au^{3+}. The dispersion color changed from brown to green indicating the formation of HGNPs. The resulting nanoparticles were washed several times by centrifugation and stored after lyophilization for further use. In the case, of TEM analyses,

17

the dispersions containing the Au NPs have been deposited on two different TEM grids: on copper carbon holey grids for some EDS and HRSTEM measurements and on Si_3N_4 membranes for the low-losses EELS analyses.

In some cases, the surface of the nanoparticles was functionalized by using SH-PEG (Methyl-polyethyleneglycol-thiol, 5KDa, Sigma-Aldrich)[38]. Poly-L-Lysine Hydrobromide (Mw: 15-30KDa, Sigma-Aldrich) was stirred during 1 h with colloidal suspensions of the HGNPs (0,5 mg/mL) in 1:1, 1:2 and 1:4 proportions to allow electrostatic attraction. Afterwards the grafted dispersions were washed repeatedly by centrifugation to remove any unbound Poly-L-Lysine. The same process was followed when using L-lysine (>98% Sigma Aldrich), Poly-D-Lysine (Mw. 1000-5000 Da, Sigma-Aldrich), BSA (>98%, Sigma Aldrich) and Poly-L-Lysine with a higher molecular weight (Mw. 1000-5000 Da).

Characterization and TEM – EELS measurements:

The mean particle size and morphology of the NIR-NPs were characterized by transmission electron microscopy (TEM) using a FEI Tecnai T20, operated at 200 kV. Zeta potential values of NPs dispersions were obtained by photon correlation spectroscopy measurements (90 Plus Brookhaven Particle Size Analyzer, Brookhaven Instruments Co, Holtsville, NY, USA).

The rest of TEM studies (EDS, HRSTEM-HAADF imaging and EELS) have been developed using a FEI Titan Low-Base microscope, working at 80 kV. This microscope is equipped with a Cs probe corrector, a monochromator and ultra-bright X-FEG electron source. For the low-loss studies, the energy resolution was below 200 meV (even 150 meV for some of the cases) and the spectra

18

were collected in STEM mode, using spectrum-image mode.[39] The convergence and collection angle were 25 and 15 mrad., respectively. The tail of the zero-loss peak has been removed using a power law subtraction method.[40]

EELS Simulations:

EELS simulations have been performed in the discrete dipole approximation (DDA) method as implemented in the DDEELS code[29,41]. The optical constant of bulk metals have been taken from tabulated data.[42] A dielectric constant of 4.20 has been taken for Si_3N_4[28,43].

19

No. 2.4520.11. The PTCI is member of the "Consortium des Équipements de Calcul Intensif (CÉCI)" (http://www.ceci-hpc.be).

Supporting Information

This material is available free of charge via the Internet at http://pubs.acs.org.

References

1.   Tsai, C. Y.; Lu, S. P.; Lin, J. W.; Lee, P. T. High Sensitivity Plasmonic Index Sensor Using Slablike Gold Nanoring Arrays. *Appl. Phys. Lett.* **2011**, 98

2.   Mahmoud, M. A.; Garlyyev, B.; El-Sayed, M. A. Determining the Mechanism of Solution Metallic Nanocatalysis with Solid and Hollow Nanoparticles: Homogeneous or Heterogeneous. *J. Phys. Chem. C* **2013**, 117, 21886-21893

3.   Gupta, S.; Stafford, R. J.; Javadi, S.; Ozkan, E.; Ensor, J. E.; Wright, K. C.; Elliot, A. M.; Jian, Y.; Serda, R. E.; Dixon, K. A.; Miller, J. J.; Klump, S.; Wallace, M. J.; Li, C. Effects of Near-infrared Laser Irradiation of Biodegradable Microspheres Containing Hollow Gold Nanospheres and Paclitaxel Administered Intraarterially in a Rabbit Liver Tumor Model. *J. Vasc. Interv. Radiol.* **2012**, 23, 553-561

4.   Timko, B. P.; Arruebo, M.; Shankarappa, S. A.; McAlvin, J. B.; Okonkwo, O. S.; Mizrahi, B.; Stefanescu, C. F.; Gomez, L.; Zhu, J.; Zhu, A.; Santamaria, J.; Langer, R.; Kohane, D. S. Near-Infrared-Actuated Devices for Remotely Controlled Drug Delivery. *P. Natl. Acad. Sci. USA* **2014**, 111, 1349-1354

5.   Lu, W.; Zhang, G. D.; Zhang, R.; Flores, L. G.; Huang, Q.; Gelovani, J. G.; Li, C. Tumor Site-Specific Silencing of NF-kappa B p65 by Targeted Hollow Gold Nanosphere-Mediated Photothermal Transfection. *Cancer Res.* **2010**, 70, 3177-3188

6.   Lu, W.; Melancon, M. P.; Xiong, C. Y.; Huang, Q.; Elliott, A.; Song, S. L.; Zhang, R.; Flores, L. G.; Gelovani, J. G.; Wang, L. H. V.; Ku, G.; Stafford, R. J.; Li, C. Effects of Photoacoustic Imaging and Photothermal Ablation Therapy Mediated by Targeted Hollow Gold Nanospheres in an Orthotopic Mouse Xenograft Model of Glioma. *Cancer Res.* **2011**, 71, 6116-6121

7.   Melancon, M. P.; Lu, W.; Yang, Z.; Zhang, R.; Cheng, Z.; Elliot, A. M.; Stafford, J.; Olson, T.; Zhang, J. Z.; Li, C. In vitro and in vivo Targeting of Hollow Gold Nanoshells Directed at Epidermal Growth Factor Receptor for Photothermal Ablation Therapy. *Mol. Cancer. Ther.* **2008**, 7, 1730-1739

20

8.	Lu, W.; Huang, Q.; Geng, K. B.; Wen, X. X.; Zhou, M.; Guzatov, D.; Brecht, P.; Su, R.; Oraevsky, A.; Wang, L. V.; Li, C. Photoacoustic Imaging of Living Mouse Brain Vasculature Using Hollow Gold Nanospheres. *Biomaterials* **2010**, 31, 2617-2626

9.	Cang, H.; Sun, T.; Li, Z. Y.; Chen, J. Y.; Wiley, B. J.; Xia, Y. N.; Li, X. D. Gold Nanocages as Contrast Agents for Spectroscopic Optical Coherence Tomography. *Opt. Lett.* **2005**, 30, 3048-3050

10.	Sebastian, V.; Lee, S. K.; Zhou, C.; Kraus, M. F.; Fujimoto, J. G.; Jensen, K. F. One-step Continuous Synthesis of Biocompatible Gold Nanorods for Optical Coherence Tomography. *Chem. Commun.* **2012**, 48, 6654-6656

11.	Tong, L.; Cobley, C. M.; Chen, J. Y.; Xia, Y. N.; Cheng, J. X. Bright Three-Photon Luminescence from Gold/Silver Alloyed Nanostructures for Bioimaging with Negligible Photothermal Toxicity. *Angew. Chem. Int. Edit.* **2010**, 49, 3485-3488

12.	Zhang, Y.; Sun, Y. J.; Liu, Z. L.; Xu, F. G.; Cui, K.; Shi, Y.; Wen, Z. W.; Li, Z. Au Nanocages for Highly Sensitive and Selective Detection of H_2O_2. *J. Electroanal. Chem.* **2011**, 656, 23-28

13.	Rycenga, M.; Wang, Z. P.; Gordon, E.; Cobley, C. M.; Schwartz, A. G.; Lo, C. S.; Xia, Y. N. Probing the Photothermal Effect of Gold-Based Nanocages with Surface-Enhanced Raman Scattering (SERS). *Angew. Chem. Int. Edit.* **2009**, 48, 9924-9927

14. Sun, Y. G.; Xia, Y. N. Shape-Controlled Synthesis of Gold and Silver Nanoparticles. *Science* **2002**, 298, 2176-2179

15. Sun, Y. G.; Mayers, B. T.; Xia, Y. N. Template-Engaged Replacement Reaction: A One-Step Approach to the Large-Scale Synthesis of Metal Nanostructures with Hollow Interiors. *Nano. Lett.* **2002**, 2, 481-485

16. Sun, Y. G.; Xia, Y. N. Mechanistic Study on the Replacement Reaction Between Silver Nanostructures and Chloroauric Acid in Aqueous Medium. *J. Am. Chem. Soc.* **2004**, 126, 3892-3901

17.	Preciado-Flores, S.; Wang, D. C.; Wheeler, D. A.; Newhouse, R.; Hensel, J. K.; Schwartzberg, A.; Wang, L. H.; Zhu, J. J.; Barboza-Flores, M.; Zhang, J. Z. Highly Reproducible Synthesis of Hollow Gold Nanospheres with Near Infrared Surface Plasmon Absorption using PVP as Stabilizing Agent. *J. Mater. Chem.* **2011**, 21, 2344-2350

18.	Edyar, J. A.; Zareie, H. M.; Blaber, M.; Dowd, A.; Cortie, M. B. Synthesis of Hollow Gold Nanoparticles and Rings Using Silver Templates. **2008** *International Conference on Nanoscience and Nanotechnology* 2008, 36-39

19.	Hakkinen, H. The Gold-Sulfur Interface at the Nanoscale. *Nat. Chem.* **2012**, 4, 443-455

20.	Grabar, K. C.; Allison, K. J.; Baker, B. E.; Bright, R. M.; Brown, K. R.; Freeman, R. G.; Fox, A. P.; Keating, C. D.; Musick, M. D.; Natan, M. J. Two-Dimensional Arrays of Colloidal Gold Particles: A Flexible Approach to Macroscopic Metal Surfaces. *Langmuir* **1996**, 12, 2353-2361

21.	Guo, L. R.; Panderi, I.; Yan, D. D.; Szulak, K.; Li, Y. J.; Chen, Y. T.; Ma, H.; Niesen, D. B.; Seeram, N.; Ahmed, A.; Yan, B. F.; Pantazatos, D.; Lu, W. A Comparative Study of Hollow Copper Sulfide Nanoparticles and Hollow Gold Nanospheres on Degradability and Toxicity. *Acs Nano* **2013**, 7, 8780-8793

22.	Goodman, A. M.; Cao, Y.; Urban, C.; Neumann, O.; Ayala-Orozco, C.; Knight, M. W.; Joshi, A.; Nordlander, P.; Halas, N. J. The Surprising in Vivo Instability of Near-IR-Absorbing Hollow Au–Ag Nanoshells. *Acs Nano* **2014**, 8, 3222-3231

21

23.   Nelayah, J.; Kociak, M.; Stephan, O.; de Abajo, F. J. G.; Tence, M.; Henrard, L.; Taverna, D.; Pastoriza-Santos, I.; Liz-Marzan, L. M.; Colliex, C. Mapping Surface Plasmons on a Single Metallic Nanoparticle. *Nat. Phys.* **2007**, 3, 348-353

24.   Arenal, R.; Stephan, O.; Kociak, M.; Taverna, D.; Loiseau, A.; Colliex, C. Electron Energy Loss Spectroscopy Measurement of the Optical Gaps on Individual Boron Nitride Single-Walled and Multiwalled Nanotubes. *Phys Rev Lett* **2005**, 95

25.   Bosman, M.; Keast, V. J.; Watanabe, M.; Maaroof, A. I.; Cortie, M. B. Mapping Surface Plasmons at the Nanometre Scale with an Electron Beam. *Nanotechnology* **2007**, 18

26.   Rossouw, D.; Couillard, M.; Vickery, J.; Kumacheva, E.; Botton, G. A. Multipolar Plasmonic Resonances in Silver Nanowire Antennas Imaged with a Subnanometer Electron Probe. *Nano. Lett.* **2011**, 11, 1499-1504

27.   Arenal, R.; Blase, X.; Loiseau, A. Boron-Nitride and Boron-Carbonitride Nanotubes: Synthesis, Characterization and Theory. *Adv Phys* **2010**, 59, 101-179

28.   Mazzucco, S.; Geuquet, N.; Ye, J.; Stephan, O.; Van Roy, W.; Van Dorpe, P.; Henrard, L.; Kociak, M. Ultralocal Modification of Surface Plasmons Properties in Silver Nanocubes. *Nano. Lett.* **2012**, 12, 1288-1294

29.   Geuquet, N.; Henrard, L. EELS and Optical Response of a Noble Metal Nanoparticle in the Frame of a Discrete Dipole Approximation. *Ultramicroscopy* **2010**, 110, 1075-1080

30.   Myroshnychenko, V.; Rodriguez-Fernandez, J.; Pastoriza-Santos, I.; Funston, A. M.; Novo, C.; Mulvaney, P.; Liz-Marzan, L. M.; de Abajo, F. J. G. Modelling the Optical Response of Gold Nanoparticles. *Chem. Soc. Rev.* **2008**, 37, 1792-1805

31.   Aizpurua, J.; Hanarp, P.; Sutherland, D. S.; Kall, M.; Bryant, G. W.; de Abajo, F. J. G. Optical Properties of Gold Nanorings. *Phys. Rev. Lett.* **2003**, 90

32.   Alali, F.; Karampelas, I. H.; Kim, Y. H.; Furlani, E. P. Photonic and Thermofluidic Analysis of Colloidal Plasmonic Nanorings and Nanotori for Pulsed-Laser Photothermal Applications. *J. Phys. Chem. C* **2013**, 117, 20178-20185

33.   Henao, J. D.; Suh, Y. W.; Lee, J. K.; Kung, M. C.; Kung, H. H. Striking Confinement Effect: AuCl4- Binding to Amines in a Nanocage Cavity. *J. Am. Chem. Soc.* **2008**, 130, 16142

34.   Tang, M. X.; Szoka, F. C. The Influence of Polymer Structure on the Interactions of Cationic Polymers with DNA and Morphology of the Resulting Complexes. *Gene. Ther.* **1997**, 4, 823-832

35.   Sun, Y. G.; Mayers, B.; Herricks, T.; Xia, Y. N. Polyol Synthesis of Uniform Silver Nanowires: A Plausible Growth Mechanism and the Supporting Evidence. *Nano Lett.* **2003**, 3, 955-960

36.   Rodriguez-Lorenzo, L.; Romo-Herrera, J. M.; Perez-Juste, J.; Alvarez-Puebla, R. A.; Liz-Marzan, L. M. Reshaping and LSPR Tuning of Au Nanostars in the Presence of CTAB. *J. Mater. Chem.* **2011**, 21, 11544-11549

37.   Prodan, E.; Radloff, C.; Halas, N. J.; Nordlander, P. A Hybridization Model for the Plasmon Response of Complex Nanostructures. *Science* **2003**, 302, 419-422

38.   von Maltzahn, G.; Park, J. H.; Agrawal, A.; Bandaru, N. K.; Das, S. K.; Sailor, M. J.; Bhatia, S. N. Computationally Guided Photothermal Tumor Therapy Using Long-Circulating Gold Nanorod Antennas. *Cancer Res.* **2009**, 69, 3892-3900

39.   Arenal, R.; de la Pena, F.; Stephan, O.; Walls, M.; Tence, M.; Loiseau, A.; Colliex, C. Extending the Analysis of EELS Spectrum-Imaging Data, from Elemental to Bond Mapping in Complex Nanostructures. *Ultramicroscopy* **2008**, 109, 32-38

40.   Egerton, R. F., *Electron Energy-Loss Spectroscopy in the Electron Microscope*. Plenum: New York, **1996**

41. http://perso.fundp.ac.be/~lhenrard/ddeels (Nov. 14th 2014)

42. Johnson P.B.; Christiy, R.W. Optical Constant of Noble Metals. *Phys. Rev. B* **1972**, 6, 4370-4379

43. "Silicon photonics. An introduction" by G.T. Reed and A.T. Knights, Willey **2004**

Graphical abstract

Morphological Tunability of the Plasmonic Response: From Hollow Gold Nanoparticles to Gold Nanorings

23

Martin Prieto, Raul Arenal*, Luc Henrard, Leyre Gomez, Victor Sebastian, Manuel Arruebo

Reshaping Hollow Gold Nanoparticles into Nanorings